Enhanced nonlinear quantum metrology with weakly coupled solitons in the presence of particle losses

Alexander Alodjants ⬤,[*] Dmitriy Tsarev ⬤, and The Vinh Ngo
Institute of Advanced Data Transfer Systems, ITMO University, Saint Petersburg 197101, Russia

Ray-Kuang Lee ⬤
Institute of Photonics Technologies, National Tsing Hua University, Hsinchu 30013, Taiwan;
Department of Physics, National Tsing Hua University, Hsinchu 30013, Taiwan;
Center for Quantum Technology, Hsinchu 30013, Taiwan;
and Physics Division, National Center for Theoretical Sciences, Taipei 10617, Taiwan

The estimation of physical parameters with Heisenberg sensitivity and beyond is one of the crucial problems for current quantum metrology. Commonly, an unavoidable lossy effect is believed to be the main obstacle when applying fragile quantum states. To utilize the lossy quantum metrology, we offer an interferometric procedure for estimation of phase parameters at the Heisenberg (up to $1/N$) and super-Heisenberg (up to $1/N^3$) scaling levels in the framework of the linear and nonlinear metrology approaches, respectively. The heart of our setup is a soliton Josephson junction (SJJ) system, which provides the formation of the quantum probe, the entangled Fock (NOON-like) state, beyond the superfluid-Mott insulator quantum phase transition point. We illustrate that such states are close to the optimal ones even with moderate losses. The enhancement of phase estimation accuracy remains feasible for both the linear and nonlinear metrologies with the SJJs and allows further improvement for the current experiments performed with atomic condensate solitons with a mesoscopic number of particles.

I. INTRODUCTION

Modern quantum technologies pose new fundamental requirements for schemes and procedures in measurement, as well as the subsequent estimation of some physical parameters in the framework of metrology and sensorics tasks [1,2]. Traditionally, such schemes are based on the interference of quantum states of light and/or matter waves [3]. In particular, the high accuracy of quantum optical measurements is paramount for the detection of gravitational waves, in which quantum states of light interfere in specially designed optical Michelson interferometers [4–6].

Although the atomic interferometers have been known for about 30 years (see, e.g., Ref. [7]), current experimental facilities open new perspectives for verification of fundamental physical laws [8–10] as well as for sensorics and metrology in real-world applications [11–14]. Typically, such facilities exploit Mach-Zehnder (MZ) interferometers based on ultracold atomic ensembles and Bose-Einstein condensates (BEC) [11,15–19]. An atomic MZ interferometer presumes certain operations (rotations) on the Bloch sphere performed with effectively two-mode atomic systems (see Fig. 3 in Ref. [1]). Experimentally, such a system may be created using atomic Josephson junctions obtained by an optical dipole trap, which provides a double-well potential for condensate atoms [20–22]. Alternatively, it is also possible to use two

hyperfine atomic states, linearly coupled by a two-photon transition [23]. In both cases, the number of condensate atoms is about a few hundred for preserving their collective behavior [24].

In this work, we examine condensate solitons for quantum metrology purposes (cf. Refs. [19,25,26]). As shown in Ref. [26], coupled solitons provide the formation of Fock states' superposition, which is close to the NOON state but behaves more robust against one-particle losses. Below we represent a comprehensive analysis of particle losses' influence on the accuracy of phase measurement and estimation performed with quantum solitons. We start from the ideal quantum metrology, which stems with the lossless limit.

The quantum approach in metrology presumes the quantum Cramér-Rao (QCR) bound for the root-mean-square error $\delta\phi$ of estimation of the arbitrary physical parameter ϕ, i.e., $\delta\phi \geqslant \frac{1}{\sqrt{\nu}\sqrt{F_Q}} \equiv \frac{\delta\phi_{\min}}{\sqrt{\nu}}$, where ν is the number of experimental runs, and F_Q is the quantum Fischer information (QFI) [27,28].

Without loss of generality, the QFI for pure states $\rho = |\Psi(\phi)\rangle\langle\Psi(\phi)|$ is defined as

$$F_Q = 4[\langle\Psi'(\phi)|\Psi'(\phi)\rangle - |\langle\Psi'(\phi)|\Psi(\phi)\rangle|^2], \quad (1)$$

where $|\Psi'(\phi)\rangle = \frac{\partial}{\partial\phi}|\Psi(\phi)\rangle$. The measurement and estimation procedure of the ϕ parameter includes some state transformations described as $|\Psi(\phi)\rangle = e^{-i\phi(\hat{b}^\dagger\hat{b})^k}|\Psi\rangle$, where k is a

---

*alexander_ap@list.ru

positive integer number, $|\Psi\rangle$ is an initial state that we prepare for the measurement, and $\hat{b}$ ($\hat{b}^\dagger$) is the annihilation (creation) operator that characterizes the quantum bosonic channel accumulating phase $\varphi \equiv \phi(\hat{b}^\dagger\hat{b})^k$.

The best precision of the measurement,

$$\delta\phi_{\min} = \frac{1}{N^k}, \qquad (2)$$

can be obtained with an ideal balanced maximally path-entangled two-mode NOON state, $|\Psi\rangle \equiv |N00N\rangle = \frac{1}{\sqrt{2}}(|N\rangle_a|0\rangle_b + |0\rangle_a|N\rangle_b)$, where N is the total average number of particles.

The Heisenberg limit (HL) for Eq. (2) is obtained in the framework of the linear metrology (LM) approach with $k = 1$. The nonlinear metrology (NLM) corresponds to the so-called super-Heisenberg limit (SHL) that may be obtained for Eq. (2) at $k \geqslant 2$ [29–33]. In particular, purely Gaussian states, or plane waves in Kerr-like medium, provide $\delta\phi_{\min} = 1/N^2$ minimal error (best accuracy) of ideal (without losses) phase estimation possessing $k = 2$ in Eq. (2). However, as we show below, quantum bright solitons potentially demonstrate a higher accuracy in the same Kerr-like medium even in the presence of losses (cf. Ref. [25]).

Losses play a decisive destructive role in the real-world implementation of quantum-metrological schemes based on nonclassical states [34]. The losses especially affect the schemes, where NOON- states are proposed to improve the parameters' estimation accuracy. As a consequence, an ideal (balanced) NOON state quickly loses the HL advantage in the phase estimation procedure even in the presence of minuscule losses in an interferometer with small particle number $N = 20$ (cf. Ref. [35]).

Entangled Fock states may be more suitable for the quantum metrology purposes in the presence of losses [36]. However, obtaining such entangled states with a relatively large number of particles is still an open problem both in theory and experiment (cf. Ref. [37]).

This work aims to demonstrate remarkable capabilities of quantum bright solitons containing a mesoscopic number of particles for both linear and nonlinear metrology problems with moderate losses occurring in appropriate MZ interferometers.

The paper is arranged as follows. In Sec. II we describe a general model of quantum bright solitons applicable for quantum metrology purposes. In Sec. III we discuss the preparation of the NOON state as a limiting one for a Fock-state superposition by means of the soliton Josephson junction (SJJ) system. We establish the conditions to obtain such a state in current experiments in the presence of one- and three-body losses. In Sec. IV we represent the analysis on a lossy MZ interferometer containing quantum bright solitons. Phase-estimation bounds with quantum solitons in the presence of losses are derived in Sec. V by means of the upper bound of Fisher information. In Sec. VI we represent our main results of quantum metrology with bright solitons. The strategies to achieve the ultimate precision in the phase estimation within a real-world experiment are discussed in detail. In Sec. VII we summarize our results and present our findings.

II. QUANTUM BRIGHT SOLITONS AS A TOOL FOR NONLINEAR METROLOGY APPLICATIONS IN THE SINGLE-MODE APPROXIMATION

In the current paper, we study the atomic BEC soliton platform. We assume that the medium supports the formation of the bright matter-wave soliton described by the wave function

$$\psi(x, t) = \frac{N\sqrt{u}}{2}\text{sech}\left[\frac{Nux}{2}\right]e^{i\frac{N^2u^2}{8}t}, \qquad (3)$$

where $\psi(x, t)$ obeys the normalization condition, $\int |\psi|^2 dx = N$, and $N = \langle\hat{N}\rangle$ is the average particle number. In Eq. (3) and thereafter we use the dimensionless parameter $u = 2\pi|a_{sc}|/a_\perp$ that characterizes Kerr-like (focusing) nonlinearity, where $a_{sc} < 0$ is the s-wave scattering length for attractive particles, $a_\perp$ is the characteristic trap scale. To be more specific in this work we discuss ^{7}Li condensates with attractive particle interaction (cf. Refs. [38–41]). Notably, the critical particle number N_c, at which the condensate collapses, is $N_c = 0.67 a_\perp/|a_{sc}|$, implying 5.2×10^3 particles in the soliton. Thereby, N_c represents the upper physical bound for the particle number that limits the quantum metrology scheme with atomic bright solitons possessing the negative scattering length.

A moderate particle number allows us to examine the single-mode approximation typically used for Gaussian wave packets [24,42,43]. Consider a classical Hamilton function,

$$H = \int dx \psi^*(x, t)\left(-\frac{1}{2}\frac{\partial^2}{\partial x^2} - \frac{u}{2}|\psi(x, t)|^2\right)\psi(x, t), \qquad (4)$$

where $\psi(x, t)$ is the wave function ansatz of the bright soliton with dimensionless variables x and t. Substituting $\psi(x, t)$ in H, one can obtain $H = -\frac{u^2}{24}N^3$.

The quantum version of the Hamilton function H is the Hamiltonian operator $\hat{H}_\phi$ that reads as

$$\hat{H}_\phi = \phi\hat{N}^3 \equiv \phi(\hat{b}^\dagger\hat{b})^3, \qquad (5)$$

where $\phi \equiv -\frac{u^2}{24}$ is the phase parameter suitable for the estimation procedure. Operators $\hat{b}$ and $\hat{b}^\dagger$ are the annihilation and creation operators characterizing soliton quantum properties in the single-mode approximation.

Thus, from Eq. (5) it is clear that instead of $k = 2$, which is valid for Gaussian states, the implementation of the quantum solitons provides the maximally accessible Kerr-like phase shift in the medium possessing degree $k = 3$ in $\hat{H}$ with respect to the particle number operator $\hat{N} = \hat{b}^\dagger\hat{b}$.

The scheme indicating the estimation procedure for the phase parameter ϕ by quantum bright solitons is plotted in Fig. 1. The procedure includes three important steps. At the first stage, we aim at the preparation of the entangled Fock (NOON-like) state $|\Psi\rangle$ that provides maximally accessible accuracy for subsequent ϕ estimation in the presence of losses. The two entangled modes here correspond to the two arms of the MZ interferometer. At the second stage, we consider the phase shift ϕ between the arms and the losses. The losses for the setup in Fig. 1 are introduced by two fictitious "beam splitters" (BSs), which provide a coupling of the setup with the environment [35,44]. At the third final step, the measurement
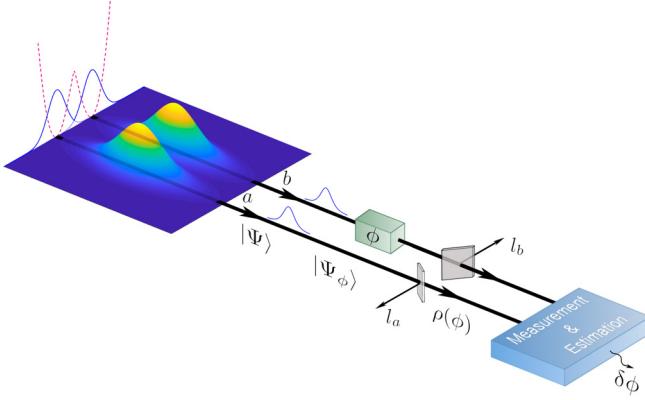
FIG. 1. Scheme of the three-step phase parameter ϕ estimation procedure with the quantum soliton Josephson junction device as an input state preparation. Possible interaction with the environment is provided by two fictitious "beam splitters" BS_a and BS_b in quantum channels a and b respectively. See the text for some details.

and ϕ-parameter estimation are performed by including ideal particle detection and outcome estimation [34].

III. QUANTUM SJJ MODEL AS A TOOL FOR STATE PREPARATION

Now, let us examine how we can prepare the entangled soliton state $|\Psi\rangle$ to achieve the maximal precision in the phase estimation, $\delta\phi_{\min}$. Here, we suggest the quantum SJJ device that represents two weakly coupled bright solitons. We assume that each of the solitons may be described in the framework of the single-mode approximation. In this limit, the Hamiltonian for the SJJ model reads as

$$\hat{H}_{\text{SJJ}} = \kappa N \Bigg\{ -\frac{\Lambda}{2}\hat{z}^2 - \frac{1}{2N}\Bigg[\sum_{k=0}^{\infty} C_{1/2}^k (-1)^k (1 - 0.21\hat{z}^2) $$
$$\times (\hat{a}^\dagger \hat{b} + \hat{b}^\dagger \hat{a})\hat{z}^{2k} + \text{H.c.} \Bigg] \Bigg\}, \quad (6)$$

where $C_{1/2}^k = \frac{1}{k!}\prod_{l=0}^{k-1}(\frac{1}{2} - l)$, $C_{1/2}^0 = 1$ are coefficients which occur from a formal Tailor expansion; $\hat{z} \equiv \frac{1}{N}(\hat{b}^\dagger\hat{b} - \hat{a}^\dagger\hat{a})$; and $\hat{a}$ and $\hat{b}$ ($\hat{a}^\dagger$ and $\hat{b}^\dagger$) are the bosonic annihilation (creation) operators for two-soliton effective modes (see Ref. [26] for details). In Eq. (6), $\Lambda \equiv u^2 N^2/16\kappa$ is a vital parameter of the SJJ system, where κ characterizes tunneling of particles between the solitons.

First, let us analyze the SJJ system without losses in general. We establish the initial state $|\Psi\rangle$ of the SJJ system in the two-mode Fock basis $|N-n\rangle_a |n\rangle_b$ as

$$|\Psi\rangle = \sum_{n=0}^{N} A_n |N-n\rangle_a |n\rangle_b, \quad (7)$$

where time-dependent coefficients A_n fulfill the stationary Schrödinger equation

$$i\frac{dA_n(\tau)}{d\tau} = \langle N-n, n|\hat{H}|\Psi(\tau)\rangle \quad (8)$$
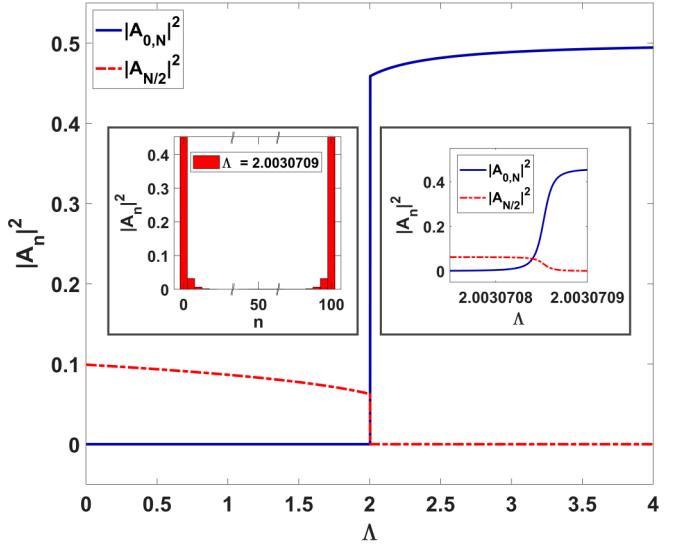
FIG. 2. Probabilities of the edge ($|A_{0,N}|^2$) and central ($|A_{N/2}|^2$) Fock modes as functions of the Λ parameter for $N = 100$ particles. The sharp phase transition at $\Lambda = \Lambda_c \simeq 2$ is shown. The right inset panel exhibits the enlarged phase transition region. The left inset panel demonstrates probabilities $|A_n|^2$ vs quantum number n for $\Lambda = 2.003\,070\,9$.

and obey the normalization condition $\sum_{n=0}^{N} |A_n|^2 = 1$; throughout this work we use effective dimensionless time $\tau = \kappa Nt$.

Substituting Eqs. (6) and (7) in Eq. (8) for unknown coefficients $A_n(\tau)$, we obtain

$$i\dot{A}_n = \alpha_n A_n + \beta_n A_{n+1} + \beta_{n-1}A_{n-1}, \quad (9)$$

where we introduce the following notations:

$$\alpha_n = -\frac{\Lambda}{2}\left(\frac{2n}{N} - 1\right)^2,$$

$$\beta_n = -\frac{1}{N^2}\Bigg(\left[1 - 0.21\left(\frac{2n}{N} - 1\right)^2\right]$$
$$\times (n+1)\sqrt{(N-n)(N-n-1)}$$
$$+ \left[1 - 0.21\left(\frac{2(n+1)}{N} - 1\right)^2\right](N-n)\sqrt{n(n+1)}\Bigg). \quad (10)$$

In this work, we find A_n numerically by considering the stationary solution of Eq. (9) with Eq. (10), which is $A_n(\tau) = A_n e^{-iE_m\tau}$, where E_m specifies the eigenenergy spectrum for Hamiltonian (6). Figure 2 demonstrates the key peculiarities for relevant probabilities $|A_n|^2$ for the system ground state, $m = 0$. With vanishing nonlinearity, i.e., for $\Lambda \simeq 0$, distribution $|A_n|^2$ approaches the Poissonian one, while the mode $|A_{N/2}|^2$ corresponds to its central peak (see the blue solid and red dashed-dotted curves in Fig. 2). The situation significantly changes in the vicinity of critical point Λ_c. The SJJ system exhibits the quantum "superfluid-Mott-insulator"-like phase transition occurring at some critical value $\Lambda_c \simeq 2$, which is shown in the right panel inset in Fig. 2. As seen from the left panel in Fig. 2, the quantum state immediately beyond phase

transition point Λ_c represents a superposition of Fock states with significantly pronounced NOON components occurring at the edges with $n = 0$ and $n = N$. Non-NOON components vanish with increasing Λ.

Thus, the state $|\Psi\rangle$ of the SJJ system for $\Lambda > \Lambda_c$ and in the absence of losses approaches the NOON state:

$$|\Psi\rangle \simeq |N00N\rangle = (|N, 0\rangle + |0, N\rangle)/\sqrt{2}. \quad (11)$$

Let us estimate how one- and three-body condensate atom losses may be important for destroying state (11). We are interested here in timescale $\tau_d = (\frac{N}{\tau_1} + \frac{N^5}{3\tau_3})^{-1}$, at which a one-particle loss event takes place in average; $\tau_1 \equiv 1/K_1$ and $\tau_3 = \frac{45a_\perp^8}{8K_3 a_{sc}^2}$ are characteristic times for one- and three-body losses possessing rates K_1 and K_3, respectively (cf. Refs. [45,46]). In the experiment reported in Ref. [38], a harmonic magneto-optical potential with characteristic frequency $\omega_\perp = 2\pi \times 710$ Hz was exploited to trap lithium condensate atoms, providing the characteristic spatial scale $a_\perp = 1.4 \times 10^{-6}$ m. Condensate bright solitons formed at the s-wave scattering length $a_{sc} = -0.21 \times 10^{-9}$ m manipulated via the Feshbach resonance technique. Coefficients K_1 and K_3 may be estimated as $K_1 = 0.05$ s^{-1} and $K_3 = 6 \times 10^{-42}$ m^6 s^{-1}, respectively (cf. Ref. [46]).

The energy-time uncertainty relation implies the additional temporal parameter $\tau_{sol} = \frac{a_\perp^2}{16\pi^2 \omega_\perp a_{sc}^2 N^2}$ for quantum solitons (cf. Refs. [45,46]); it characterizes the timescale at which a quantum soliton occurs. Obviously, in adiabatic approximation $\tau_{sol} \ll \tau_d$, and decoherence processes are slow enough to keep the soliton-shape envelope.

For mesoscopic particle number $N \simeq 100$ we estimate characteristic timescales as $\tau_d \simeq 200$ ms and $\tau_{sol} = 6.3$ ms, respectively. Noteworthy, in this limit the three-particle losses' contribution in τ_d is negligibly small. Our estimations show that such losses become important for particle number $N \geqslant 3000$ (cf. Ref. [46]). However, macroscopically large N leads to the collapse of the soliton.

Thus, two tunnel-coupled bright solitons with the mesoscopic number of particles are suitable to create the superposition NOON-like state $|\Psi\rangle$ within appropriate timescales

$$\tau_{sol} < \tau \ll \tau_d. \quad (12)$$

Inequalities (12) represent the conditions necessary to obtain the HL and/or the SHL for the quantum metrology scheme in Fig. 1, operating with quantum solitons in the framework of LM and NLM, respectively.

IV. SOLITON-BASED INTERFEROMETER WITH LOSSES

Consider the scheme of quantum metrology plotted in Fig. 1 in the presence of particle losses. For our purposes we take state (7) as initial and then take into account the losses in two arms of the interferometer via the fictitious BS approach. This approach represents a powerful tool for modeling the coupling of quantum macroscopic superposition states with the environment (cf. Refs. [35,47]). After two BSs the "input" two-mode Fock state in Eq. (7) transforms into (cf. Ref. [47])

$$|N - n\rangle_a |n\rangle_b \rightarrow \sum_{l_b=0}^{N} \sum_{l_a=0}^{N-l_b} \sqrt{B_{l_a,l_b}^n} |N - n - l_a\rangle_a |n - l_b\rangle_b |l_a\rangle |l_b\rangle, \quad (13)$$

where l_a and l_b are the numbers of particles lost from the a and b channels, respectively. In Eq. (13) we also introduce the coefficient

$$B_{l_a,l_b}^n = \binom{N-n}{l_a} \binom{n}{l_b} \eta_a^{N-n} (\eta_a^{-1} - 1)^{l_a} \eta_b^n (\eta_b^{-1} - 1)^{l_b}, \quad (14)$$

where η_a and η_b ($\eta_{a,b} \leqslant 1$) are the transmissivities of BSs in channels a and b, respectively. We examine the physically identical arms a and b of the interferometer by setting $\eta \equiv \eta_a \simeq \eta_b$.

To take into account the phase shift ϕ in Fig. 1, we apply the transformation $\hat{U}_\phi$ to state (7), which leads to the replacement $|N - n\rangle_a |n\rangle_b \rightarrow e^{in^k \phi} |N - n\rangle_a |n\rangle_b$. Then, we can represent the density matrix ρ for the final state after particle losses as

$$\rho = \sum_{l_b=0}^{N} \sum_{l_a=0}^{N-l_b} p_{l_a,l_b} |\xi\rangle\langle\xi|, \quad (15)$$

where

$$|\xi\rangle = \frac{1}{\sqrt{p_{l_a,l_b}}} \sum_{n=l_b}^{N-l_a} C_{l_a,l_b}^n e^{in^k \phi} |N - n - l_a\rangle_a |n - l_b\rangle_b \quad (16)$$

is one of the possible pure states of the system after l_a and l_b particle losses; and $p_{l_a,l_b} = \sum_{n=l_b}^{N-l_a} (C_{l_a,l_b}^n)^2 \equiv \sum_{n=l_b}^{N-l_a} A_n^2 B_{l_a,l_b}^n$ is a normalization factor. Here, we have no interest in the lost particles; for simplicity, in Eq. (15) we have traced out modes $|l_a\rangle|l_b\rangle$.

It is instructive to examine the influence of particle losses occurring before the phase ϕ creation (cf. Fig. 1). In other words, we examine how the ideal NOON state (11) degrades in the interferometer without any phase accumulation. In this limit, we formally suppose $k = 0$ in Eq. (16); the coefficients approach

$$A_n = \begin{cases} \frac{1}{\sqrt{2}}, & \text{if } n = 0, N; \\ 0, & \text{if } 0 < n < N. \end{cases} \quad (17)$$

Substituting Eq. (17) in Eq. (15), one can obtain the density matrix for the NOON state after losses as

$$\rho = \eta^N |N00N\rangle\langle N00N| + \frac{1}{2} \sum_{l_a=1}^{N} B_{l_a,0}^0 |N - l_a, 0\rangle\langle N - l_a, 0|$$

$$+ \frac{1}{2} \sum_{l_b=1}^{N} B_{0,l_b}^N |0, N - l_b\rangle\langle 0, N - l_b|. \quad (18)$$

Then, taking into account Eq. (14) one can write

$$\rho = \eta^N |N00N\rangle\langle N00N| + \frac{1}{2} \sum_{n_a=0}^{N-1} p_{n_a} |n_a, 0\rangle\langle n_a, 0|$$

$$+ \frac{1}{2} \sum_{n_b=0}^{N-1} p_{n_b} |0, n_b\rangle\langle 0, n_b|, \quad (19)$$

where $n_a = N - l_a$ and $n_b = N - l_b$ are the numbers of particles remaining in the arms of the interferometer and

$$p_n = \binom{N}{n} \eta^n (1 - \eta)^{N-n} \quad (20)$$

is a binomial distribution function of the density matrix diagonal elements.

As seen from Eq. (19), the particle losses transform the NOON state into a two-mode Fock states mixture with binomial distribution (20). Notice, in Eq. (19) only the term with $n = N$ (the case when no particles are lost) is maximally path entangled. For $\eta \to 1$ and $N \gg 1$ and finite $N(1 - \eta)$, the binomial distribution (20) can be approximated by the Poissonian one

$$p_n^{\text{Poisson}} = \frac{[N(1 - \eta)]^{N-n}}{(N - n)!} e^{-N(1-\eta)}. \qquad (21)$$

Finally, at $N(1 - \eta) \gg 1$ one can use the approximation of Eq. (21) by the Gaussian distribution

$$p_n^{\text{Gauss}} = \frac{1}{\sqrt{2\pi N(1 - \eta)}} e^{-\frac{(n-N\eta)^2}{2N(1-\eta)}}. \qquad (22)$$

The distribution in Eq. (22) possesses width $2\sigma = 2\sqrt{N(1 - \eta)}$ with mean particle number $\bar{n} = N\eta$. For example, if $N = 100$ and $\eta = 0.8$, then $\bar{n} = 80$ and $2\sigma \approx 9$.

Thus, in the presence of losses, the particle number distributions are broadened [see Eqs. (11)–(22)]. Obvious arguments tell us that the broadening of the particle number distribution negatively affects the accuracy of the ϕ-phase-parameter measurement. Actually, the uncertainty in the phase parameter estimation occurs due to the quantum-mechanical fluctuations in the particle number difference $\delta\phi \simeq \langle[\Delta(N_a - N_b)]^2\rangle^{-1/2}$. In this case, we obtain $\delta\phi = \{N[1 + \eta(N\eta - 1)]\}^{-1/2}$. Without any losses (for $\eta = 1$), $\delta\phi$ approaches $1/N$, corresponding to the HL accuracy.

V. PHASE ESTIMATION BOUNDS WITH QUANTUM SOLITONS

Now let us analyze the case when losses occur after the phase accumulation. We examine the QFI, F_Q, in the presence of losses for the setup in Fig. 1. In particular, accounting in Eq. (15) for the density matrix representation in the diagonal form $\rho = \sum_{i=1}^{s} \lambda_i |\psi_i\rangle\langle\psi_i|$, where λ_i and $|\psi_i\rangle$ are eigenvalues and eigenstates of ρ, respectively (s is the rank), we can establish the QFI as (cf. Refs. [48,49])

$$F_Q = \sum_{i=1}^{s} \left[\frac{1}{\lambda_i} \left(\frac{\partial\lambda_i}{\partial\phi} \right)^2 + 4\lambda_i\langle\psi_i'|\psi_i'\rangle \right.$$
$$\left. - \sum_{j=1}^{s} \frac{8\lambda_i\lambda_j}{\lambda_i + \lambda_j} |\langle\psi_i|\psi_j'\rangle|^2 \right], \qquad (23)$$

where $|\psi_i'\rangle \equiv \frac{\partial}{\partial\phi} |\psi_i\rangle$.

Numerical calculation of the QFI defined in Eq. (23) and performed in the case of the NLM for large N represents a nontrivial computational task. In this work, we restrict ourselves by studying only the upper bound of the QFI, denoted as $\tilde{F}_Q$ ($F_Q \leqslant \tilde{F}_Q$), which reads as

$$\tilde{F}_Q = \sum_{l_b=0}^{N} \sum_{l_a=0}^{N-l_b} p_{l_a,l_b} F_Q[|\xi(\phi)\rangle\langle\xi(\phi)|], \qquad (24)$$

where $F_Q[|\xi(\phi)\rangle\langle\xi(\phi)|]$ is Eq. (1) with the state defined in Eq. (16). Then, substituting Eq. (16) in Eq. (24) for the upper

bound of the QFI $\tilde{F}_Q$, we obtain

$$\tilde{F}_Q = 4 \left[\sum_{n=0}^{N} n^{2k} A_n^2 - \sum_{l_b=0}^{N} \sum_{l_a=0}^{N-l_b} \frac{\left(\sum_{n=l_b}^{N-l_a} n^k C_{l_a,l_b}^n{}^2 \right)^2}{\sum_{n=l_b}^{N-l_a} C_{l_a,l_b}^n{}^2} \right], \qquad (25)$$

where A_n is the C_{l_a,l_b}^n coefficient taken at $l_a, l_b = 0$ [35,47].

Notice that for the pure states used in Eqs. (24) and (25) we have $F_Q = \tilde{F}_Q$.

Let us estimate the upper bound of the QFI for density matrix (15) and suppose that the NOON state

$$|N00N\rangle = (|N, 0\rangle + e^{in^k\phi}|0, N\rangle)/\sqrt{2} \qquad (26)$$

occurs before the particle losses, as shown in Fig. 1. We can still use Eq. (19) for the density matrix but with Eq. (26). In this limit the first term in Eq. (19) contains the off-diagonal elements carrying the information about the ϕ parameter. At the same time, the sum in Eq. (19) consists only of the main-diagonal elements. This occurs due to the initially maximal entangled NOON state collapsing into a Fock state, when a single particle is lost (cf. Ref. [35]). The QFI upper bound (25) in this case reads as

$$\tilde{F}_Q = N^{2k}\eta^N. \qquad (27)$$

Equation (27) allows us to estimate the initial total particle number, $N_{\min}$, which provides the minimal error for the ϕ measurement with the NOON state in the presence of losses. Such precision requires the maximal value of $\tilde{F}_Q$ that we can find from the condition $\partial\tilde{F}_Q/\partial N = 0$. In this case, from Eq. (27) we obtain the equation for $N_{\min}$:

$$N_{\min} = -\frac{2k}{\ln\eta}. \qquad (28)$$

For example, for the lossy interferometer with $\eta = 0.9$, Eq. (28) provides limitations for the particle numbers $N_{\min} \simeq 19$ and $N_{\min} \simeq 57$ for $k = 1$ and $k = 3$, respectively (cf. Ref. [35]).

Equation (27) also provides the precision of the phase estimation:

$$\delta\phi_\eta = \frac{1}{\sqrt{\eta^N} N^k} \qquad (29)$$

with the input NOON state in the presence of losses. As seen from Eq. (29), at $\eta \to 1$, $\delta\phi_\eta$ reaches the HL, $\delta_{\text{HL}} = 1/N$, and the SHL, $\delta_{\text{SHL}} = 1/N^3$, for $k = 1$ and $k = 3$, respectively.

On the other hand, the standard interferometric limit (SIL) for the setup in Fig. 1 may be obtained numerically by means of the binomial distributed initial state

$$|\Psi\rangle = \frac{1}{\sqrt{2^N}} \sum_{n=0}^{N} \sqrt{\binom{N}{n}} e^{i\phi n^k} |N - n\rangle_a |n\rangle_b. \qquad (30)$$

In the presence of losses for Eq. (30) one can obtain

$$\delta\phi_k \propto \frac{1}{\sqrt{\eta} N^{k-1/2}}. \qquad (31)$$

The numerical simulations reveal that for $k = 1$ Eq. (31) matches the SIL, $\delta\phi_1 = \delta\phi_{\text{SIL}} \equiv 1/\sqrt{\eta N}$ (cf. Ref. [47]).

Similarly, one can define the nonlinear interferometric limit (NIL), $\delta\phi_{\text{NIL}}$, which occurs in the framework of the nonlinear metrology approach. Setting $k = 3$ in Eq. (25) for
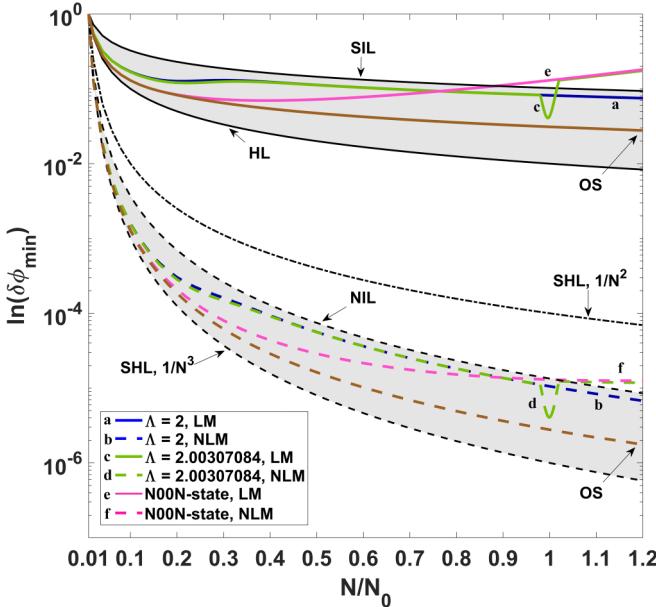
FIG. 3. The logarithmic plot of the best accuracy $\delta\phi_{\min}$ for the phase estimation based on the SJJ as a function of normalized number of particles N/N_0. The parameters used are $N_0 = 100$ and $\eta_a = \eta_b = 0.95$. The upper shadow region depicts the area between the SIL and the HL for $k = 1$. The lower shadow region corresponds to the area between the NIL and the SHL at $k = 3$ [see Eq. (2)]. See more details in the text.

FIG. 4. The best accuracy $\delta\phi_{\min}$ of the phase estimation based on the SJJ vs transmissivity $\eta_a = \eta_b \equiv \eta$ of the fictitious BSs for the linear metrology ($k = 1$) and the nonlinear one (the inset, $k = 3$) with $N = 100$ particles. See more details in the text.

the coherent atomic wave packets, we can obtain $\delta\phi_{\mathrm{NIL}} = 1/\sqrt{\eta N^5}$.

VI. DISCUSSION

In Figs. 3 and 4 we demonstrate the main results of our work. The curves (a)–(f) correspond to the phase estimation procedure performed with the quantum state initially prepared by SJJ (cf. Fig. 1). The curves (a) and(b) and the curves (e), and (f) correspond to the SJJ Λ parameter chosen before and after the phase transition point, respectively. The curves (c) and (d) in Figs. 3 and 4 characterize the SJJ system at the phase transition point $\Lambda = \Lambda_c = 2.003\,070\,84$.

In Fig. 3 we establish the minimal error (maximal accuracy) for the phase estimation (represented in the logarithmic scale) as a function of the normalized particle number N. The upper (solid) curves correspond to the LM limit obtained at $k = 1$ with Eq. (25).

The upper black line in Fig. 3 corresponds to the SIL and characterizes the phase estimation procedure with the initially prepared coherent atomic wave packets. The SIL reads as $\delta\phi_{\mathrm{SIL}} = 1/\sqrt{\eta N}$; it can be obtained from Eq. (25) at $k = 1$ and represents the generalization of the SQL in the presence of particle losses (see Eq. (30), cf. Ref. [47]). Similar behavior is inherent to the lower shadow region in Fig. 3.

The nonlinear phase estimation with solitons is established by the lower (dashed) curves plotted at $k = 3$. The intermediate (black dashed) curve establishes the SHL $\propto 1/N^2$ obtained with $k = 2$. These limits are discussed in Ref. [29] and correspond to the phase estimation by means of usual Kerr-like medium with plane waves. The SJJ environment generates

a two-mode Fock state with a particular superposition given by coefficients A_n that are Λ parameter dependent. For the optimal state (OS, the brown curve in Fig. 3), we numerically optimize the QFI upper bound $\tilde{F}_Q$ (25) over all such two-mode Fock-state superpositions (cf. Ref. [35]).

Figure 3 exhibits two important features, which are relevant to the quantum metrology performed with bright solitons. First, the absolute value of phase estimation accuracy is minimal with the coupled solitons even in the presence of losses and for coherent probes [see the blue dashed curve (b) in Fig. 3] compared to other currently available metrological approaches beyond the HL (see the lower shadow region in Fig. 3 and cf. Ref. [29]).

Second, the phase estimation with the initially prepared SJJ system establishes the best accuracy for both linear and nonlinear metrological purposes in comparison with the NOON state, which we depict by the magenta curves (e) and (f) in Fig. 3. The capability of the SJJ system as a probe-state preparation device for the phase estimation procedure we establish by the green curves (c) and (d) in Fig. 3, which correspond to the phase transition point $\Lambda = \Lambda_c = 2.003\,070\,84$ with $N = N_0$ particles. Moreover, the minimal value of the estimated phase parameter is close to the results obtained with the OS. A particular value of N_0 is determined from the experimental facilities, which are used for the SJJ device design. The particle number involved in Fig. 3 is assumed to be $N_0 = 100$.

In Fig. 4, we represent the accuracy $\delta\phi_{\min} = \tilde{F}_Q^{-1/2}$ vs the channel transmissivity, η parameter, for the linear ($k = 1$) and nonlinear ($k = 3$) metrology phase estimation procedures, respectively. The NLM peculiarities are given in the inset of Fig. 4.

At $\eta = 1$ all the curves start at the points representing the accuracy of the lossless metrology with the SJJs at the

correspondent Λ. For the SJJ device in the Mott-insulator regime, at $\Lambda \geqslant 2.1$, the accuracies of the linear and nonlinear metrology match the HL ($\delta\phi_{\min} = 1/N$) and the SHL ($\delta\phi_{\min} = 1/N^3$), respectively. In the presence of losses, $\delta\phi_{\min}$ grows depending on the value of the Λ parameter, which is relevant to the performance of the SJJs as a device for the probe-state preparation in Fig. 1. The curves with various Λ in Fig. 4 correspond to the crossover region from the superfluid ($\Lambda = 2$) to the Mott-insulator ($\Lambda = 2.1$) regimes that take place in the SJJ system.

Remarkably, in the LM case the difference between F_Q and $\tilde{F}_Q$ for the SJJ model is more than satisfactory, excluding the phase transition point. Only less than 0.5% discrepancy can be seen before the phase transition and less than 4% after the phase transition. At the phase transition point, the difference between F_Q and $\tilde{F}_Q$ reaches 60%. In the presence of losses it happens in the vicinity of the inflection point with $\eta \lesssim 0.9$ (see Fig. 4). At this point, F_Q behaves more sharply than $\tilde{F}_Q$. Notice, the plots in Fig. 3 are represented for $\eta = 0.95$, which corresponds to the vanishing discrepancy between F_Q and $\tilde{F}_Q$.

From the blue (a) and red (b) curves in Fig. 4, it is clearly seen that at moderate values of η the phase estimation accuracy approaches $\delta\phi_{\text{SIL}}$ for the SJJ system close to the superfluid regime, $\Lambda < \Lambda_c$. The behavior of $\delta\phi_{\min}$ beyond critical point $\Lambda \geqslant \Lambda_c$ is determined by the properties of entangled Fock states at the input of the setup in Fig. 1 in the presence of losses. Even at $\Lambda = 2.1$ [see the magenta (e) curve in Fig. 4], accuracy $\delta\phi_{\min}$ approaches the one obtained for the ideal NOON state, $\delta\phi_{\min} = \delta\phi_\eta = 1/N^k\eta^{N/2}$ [see Eq. (31)].

Strictly speaking, using such states in metrology is justified (for a given particle number N) if the transmissivity of quantum channels satisfies the condition [cf. Eq. (27)]

$$\eta \geqslant \eta_c \equiv e^{-2k/N}. \tag{32}$$

Thus, inequality (32) represents a condition sufficient for the improvement of phase estimation in the quantum metrology scheme (Fig. 1) with the NOON state obtained with the SJJ system.

Notably, in the presence of significant losses ($\eta \ll \eta_c$) entangled Fock or NOON states are not applicable, and the spin-squeezed states with $\Lambda < \Lambda_c$ demonstrate the accuracy better than the SIL. The best accuracy for $\eta < 0.9$ is provided by the borderline state with $\Lambda = \Lambda_c$ due to the existence of planar spin-squeezing in the entangled Fock modes (cf. Ref. [26]) [see the green (c) curve in Fig. 4].

In Fig. 4, we also compare the results with the OS (the brown dotted curves). As seen, the results with the OS and the states provided by the SJJ are close to each other in the regions with $0 < \eta \leqslant 0.3$ and $0.9 < \eta \leqslant 1$, which correspond to the high and low losses limits, respectively. The difference between the optimal and SJJ states is notable at

intermediate values of η close to the inflection points (see Fig. 4). Such a behavior takes place due to the phase transition effect that occurs abruptly and evokes a rapid quantum state transformation.

VII. CONCLUSION

By utilizing the soliton Josephson Junction system as a quantum probe, we propose the interferometric procedure for the appropriate phase parameters' estimation at the Heisenberg (up to $1/N$) and the practically unique super-Heisenberg (up to $1/N^3$) scaling levels in the framework of linear and nonlinear metrology approaches, respectively. Counterintuitively, operating near the quantum phase transition point helps to sustain the accuracy of the phase estimation even in the presence of particle losses. In particular, we account for the influence of losses at three different steps for the setup proposed in Fig. 1. The necessary and sufficient conditions are established for the parameter estimation accuracy improvement with the SJJ system in the framework of the linear and nonlinear metrology tasks. For the lossy quantum metrology scheme, the effect of coupling with the environment causes some number of particles to be removed from each quantum channel introducing extra (vacuum) noises. We model these losses by means of the fictitious BS approach that presumes transmissivities of a and b channels characterized by parameters η_a and η_b ($\eta_{a,b} \leqslant 1$), respectively. Further, we suppose that channels a and b are physically equivalent and $\eta_a \simeq \eta_b = \eta$. The resulting quantum state in the lossy channel is a mixed state described by the density matrix. With the QFI, we reveal the main features of such a quantum metrology. We have shown that the particle number is crucial for the superposition state formation and for the critical value of BSs' transmissivity η_c. In particular, practically reasonable values of η_c requires a few hundreds of particles per soliton and less. We have demonstrated that in this case it is feasible to create NOON-like states which, then, may be used for phase measurement and estimation procedures. In this sense, our results contribute to further improvement of the current experiments performed with atomic condensate solitons containing a mesoscopic number of particles.

[1] L. Pezzè, A. Smerzi, M. K. Oberthaler, R. Schmied, and P. Treutlein, Quantum metrology with nonclassical states of atomic ensembles, Rev. Mod. Phys. **90**, 035005 (2018).

[2] C. L. Degen, F. Reinhard, and P. Cappellaro, Quantum sensing, Rev. Mod. Phys. **89**, 035002 (2017).

[3] J. P. Dowling and K. P. Seshadreesan, Quantum optical technologies for metrology, sensing, and imaging, J. Lightwave Technol. **33**, 2359 (2015).

[4] J. Aasi, J. Abadie, B. Abbott *et al.*, Enhanced sensitivity of the LIGO gravitational wave detector by using squeezed states of light, Nat. Photon. **7**, 613 (2013).

[5] Y. Zhao, N. Aritomi, E. Capocasa, M. Leonardi, M. Eisenmann, Y. Guo, E. Polini, A. Tomura, K. Arai, Y. Aso, Y. C. Huang, R. K. Lee, H. Luck, O. Miyakawa, P. Prat, A. Shoda, M. Tacca, R. Takahashi, H. Vahlbruch, M. Vardaro *et al.*, Frequency-Dependent Squeezed Vacuum Source for Broadband Quantum Noise Reduction in Advanced Gravitational-Wave Detectors, Phys. Rev. Lett. **124**, 171101 (2020).

[6] L. McCuller, C. Whittle, D. Ganapathy, K. Komori, M. Tse, A. Fernandez-Galiana, L. Barsotti, P. Fritschel, M. MacInnis, F. Matichard, K. Mason, N. Mavalvala, R. Mittleman, H. Yu, M. E. Zucker, and M. Evans, Frequency-Dependent Squeezing for Advanced LIGO, Phys. Rev. Lett. **124**, 171102 (2020).

[7] M. Kasevich and S. Chu, Atomic Interferometry Using Stimulated Raman Transitions, Phys. Rev. Lett. **67**, 181 (1991).

[8] D. N. Aguilera, H. Ahlers, B. Battelier, A. Bawamia *et al.*, STE-QUEST—test of the universality of free fall using cold atom interferometry, Class. Quantum Grav. **31**, 115010 (2014).

[9] H. Muntinga, H. Ahlers, M. Krutzik, A. Wenzlawski, S. Arnold, D. Becker, K. Bongs, H. Dittus, H. Duncker, N. Gaaloul, C. Gherasim, E. Giese, C. Grzeschik, T. W. Hansch, O. Hellmig, W. Herr, S. Herrmann, E. Kajari, S. Kleinert, C. Lammerzahl *et al.*, Interferometry with Bose-Einstein Condensates in Microgravity, Phys. Rev. Lett. **110**, 093602 (2013).

[10] M. D. Lachmann, H. Ahlers, D. Becker *et al.*, Ultracold atom interferometry in space, Nat. Commun. **12**, 1317 (2021).

[11] K. Bongs, M. Holynski, J. Vovrosh *et al.*, Taking atom interferometric quantum sensors from the laboratory to real-world applications, Nat. Rev. Phys. **1**, 731 (2019).

[12] R. Geiger, V. Ménoret, G. Stern *et al.*, Detecting inertial effects with airborne matter-wave interferometry, Nat. Commun. **2**, 474 (2011).

[13] A. Hinton, M. Perea-Ortiz, J. Winch *et al.*, A portable magneto-optical trap with prospects for atom interferometry in civil engineering, Philos. Trans. R. Soc., A **375**, 20160238 (2017).

[14] Y. Bidel, N. Zahzam, C. Blanchard *et al.*, Absolute marine gravimetry with matter-wave interferometry, Nat. Commun. **9**, 627 (2018).

[15] C. Gross, T. Zibold, E. Nicklas, J. Esteve, and M. K. Oberthaler, Nonlinear atom interferometer surpasses classical precision limit, Nature (London) **464**, 1165 (2010).

[16] D. Becker, M. D. Lachmann, S. T. Seidel *et al.*, Space-borne Bose–Einstein condensation for precision interferometry, Nature (London) **562**, 391 (2018).

[17] H. Lee, P. Kok, and J. P. Dowling, A quantum Rosetta stone for interferometry, J. Mod. Opt. **49**, 2325 (2002).

[18] M. Hauth, C. Freier, V. Schkolnik, A. Peters, H. Wziontek, and M. Schilling, Atom interferometry for absolute measurements of local gravity, in *Proceedings of the International School of Physics "Enrico Fermi"* (IOS, Amsterdam, 2014), Vol. 188, pp. 557–603.

[19] D. V. Tsarev, S. M. Arakelyan, Y.-L. Chuang, R.-K. Lee, and A. P. Alodjants, Quantum metrology beyond Heisenberg limit with entangled matter wave solitons, Opt. Express **26**, 19583 (2018).

[20] R. Gati, M. Albiez, J. Fölling *et al.*, Realization of a single Josephson junction for Bose–Einstein condensates, Appl. Phys. B **82**, 207 (2006).

[21] M. Albiez, R. Gati, J. Fölling, S. Hunsmann, M. Cristiani, and M. K. Oberthaler, Direct Observation of Tunneling and Non-linear Self-Trapping in a Single Bosonic Josephson Junction, Phys. Rev. Lett. **95**, 010402 (2005).

[22] G. Mazzarella, L. Salasnich, A. Parola, and F. Toigo, Coherence and entanglement in the ground state of a bosonic Josephson junction: From macroscopic Schrödinger cat states to separable Fock states, Phys. Rev. A **83**, 053607 (2011).

[23] W. Muessel, H. Strobel, D. Linnemann, T. Zibold, B. Julia-Diaz, and M. K. Oberthaler, Twist-and-turn spin squeezing in Bose-Einstein condensates, Phys. Rev. A **92**, 023603 (2015).

[24] J. R. Anglin and A. Vardi, Dynamics of a two-mode Bose-Einstein condensate beyond mean-field theory, Phys. Rev. A **64**, 013605 (2001).

[25] D. V. Tsarev, T. V. Ngo, R.-K. Lee, and A. P. Alodjants, Nonlinear quantum metrology with moving matter-wave solitons, New J. Phys. **21**, 083041 (2019).

[26] D. V. Tsarev, A. P. Alodjants, T. V. Ngo, and R.-K. Lee, Mesoscopic quantum superposition states of weakly-coupled matter-wave solitons, New J. Phys. **22**, 113016 (2020).

[27] G. Tóth and I. Apellaniz, Quantum metrology from a quantum information science perspective, J. Phys. A: Math. Theor. **47**, 424006 (2014).

[28] R. Demkowicz-Dobrzański, M. Jarzyna, and J. Kołodyński, Quantum limits in optical interferometry, Prog. Opt. **60**, 345 (2015).

[29] D. Maldonado-Mundo and A. Luis, Metrological resolution and minimum uncertainty states in linear and nonlinear signal detection schemes, Phys. Rev. A **80**, 063811 (2009).

[30] M. Beau and A. del Campo, Nonlinear Quantum Metrology of Many-Body Open Systems, Phys. Rev. Lett. **119**, 010403 (2017).

[31] M. Napolitano and M. W. Mitchell, Nonlinear metrology with a quantum interface, New J. Phys. **12**, 093016 (2010).

[32] J. Cheng, Quantum metrology for simultaneously estimating the linear and nonlinear phase shifts, Phys. Rev. A **90**, 063838 (2014).

[33] A. Luis, Quantum limits, nonseparable transformations, and nonlinear optics, Phys. Rev. A **76**, 035801 (2007).

[34] N. Thomas-Peter, B. J. Smith, A. Datta, L. Zhang, U. Dorner, and I. A. Walmsley, Real-World Quantum Sensors: Evaluating Resources for Precision Measurement, Phys. Rev. Lett. **107**, 113603 (2011).

[35] U. Dorner, R. Demkowicz-Dobrzanski, B. J. Smith, J. S. Lundeen, W. Wasilewski, K. Banaszek, and I. A. Walmsley, Optimal Quantum Phase Estimation, Phys. Rev. Lett. **102**, 040403 (2009).

[36] S. D. Huver, C. F. Wildfeuer, and J. P. Dowling, Entangled Fock states for robust quantum optical metrology, imaging, and sensing, Phys. Rev. A **78**, 063828 (2008).

[37] T. V. Ngo, D. V. Tsarev, Ray-Kuang Lee, and A. P. Alodjants, Bose–Einstein condensate soliton qubit states for metrological applications, Sci. Rep. **11**, 19363 (2021).

[38] L. Khaykovich, F. Schreck, G. Ferrari, T. Bourdel, J. Cubizolles, L. D. Carr, Y. Castin, and C. Salomon, Formation of a matter-wave bright soliton, Science **296**, 1290 (2002).

[39] J. H. Nguyen, P. Dyke, D. Luo, B. A. Malomed, and R. G. Hulet, Collisions of matter-wave solitons, Nat. Phys. **10**, 918 (2014).

[40] P. G. Kevrekidis, D. J. Frantzeskakis, and R. Carretero-González, *Emergent Nonlinear Phenomena in Bose–Einstein Condensates* (Springer-Verlag, Berlin, 2008).

[41] K. E. Strecker, G. B. Partridge, A. G. Truscott, and R. G. Hulet, Formation and propagation of matter-wave soliton trains, Nature (London) **417**, 150 (2002).

[42] A. S. Parkins and D. F. Walls, The physics of trapped dilute-gas Bose–Einstein condensates, Phys. Rep. **303**, 1 (1998).

[43] J. I. Cirac, M. Lewenstein, K. Mølmer, and P. Zoller, Quantum superposition states of Bose-Einstein condensates, Phys. Rev. A **57**, 1208 (1998).

[44] M. Bohmann, J. Sperling, and W. Vogel, Entanglement and phase properties of noisy NOON states, Phys. Rev. A **91**, 042332 (2015).

[45] C. Weiss, S. A. Gardiner, and H. P. Breuer, From short-time diffusive to long-time ballistic dynamics: The unusual center-of-mass motion of quantum bright solitons, Phys. Rev. A **91**, 063616 (2015).

[46] C. Weiss, S. L. Cornish, S. A. Gardiner, and H. P. Breuer, Superballistic center-of-mass motion in one-dimensional attractive Bose gases: Decoherence-induced Gaussian random walks in velocity space, Phys. Rev. A **93**, 013605 (2016).

[47] R. Demkowicz-Dobrzanski, U. Dorner, B. J. Smith, J. S. Lundeen, W. Wasilewski, K. Banaszek, and I. A. Walmsley, Quantum phase estimation with lossy interferometers, Phys. Rev. A **80**, 013825 (2009).

[48] J. Liu, X.-X. Jing, W. Zhong, and X.-G. Wang, Quantum Fisher information for density matrices with arbitrary ranks, Commun. Theor. Phys. **61**, 45 (2014).

[49] S. L. Braunstein and C. M. Caves, Statistical Distance and the Geometry of Quantum States, Phys. Rev. Lett. **72**, 3439 (1994).